Adaptive Airborne Ionospheric Gradient Monitoring for Dual-Frequency GBAS

Daniel Gerbeth, Maria Caamano, *German Aerospace Center (DLR)*

BIOGRAPHIES

Daniel Gerbeth received his Bachelor's and Master's degrees in Electrical Engineering and Information Technology from the Karlsruhe Institute of Technology, Germany, in 2014. During his master studies he specialized in aerospace technology and navigation. After working in the field of sensor fusion and navigation aiding at Fraunhofer IOSB, he joined the German Aerospace Center (DLR) in May 2015 and has since been involved in research on Ground Based Augmentation Systems (GBAS) and reliable navigation for urban air mobility.

Maria Caamano received a Master's degree in Telecommunications engineering from the University of Oviedo, Spain, in March 2015, and a PhD in Aerospace Science and Technology from the Polytechnic University of Catalonia (UPC), Spain, in July 2022. Since May 2015, she has been working as a research associate at the Institute of Communications and Navigation at the German Aerospace Center (DLR). Her work focuses on the development of dual-frequency multi-constellation Ground Based Augmentation Systems (GBAS).

ABSTRACT

This work proposes a new method for detecting ionospheric activity in the context of future dual-frequency Ground Based Augmentation Systems (GBAS). We utilize measurements available to an airborne GBAS user to derive a probability for large anomalous ionospheric gradients currently present between the aircraft and the local GBAS station. For this purpose, two metrics in satellite range domain are introduced for activity detection: the first is based on the total ionospheric delay difference between ground and air and the second one uses a cumulative sum (CUSUM) based monitoring approach of the rate of change of ionospheric delay difference estimates.

After introducing the new concept for this ionospheric activity monitoring, we explain the design parameters that influence the sensitivity of the test and how they can be adjusted. Based on a large simulation dataset, we evaluate the detection capability of the new approach and subsequently the potential to reduce the ionospheric protection levels under nominal conditions by ensuring the absence of harmful ionospheric disturbances. Finally, the monitoring is applied to a measurement dataset within an experimental GBAS facility to evaluate the potential to improve monitor performance and thus improve nominal availability in the presence of significant local multipath. Overall, the results indicate the potential to improve system availability, especially in situations where few satellites are available, such as when using a single constellation, while being able to detect ionospheric activity before the onset of harmful errors for an airborne GBAS user on approach.

1. INTRODUCTION

The Ground Based Augmentation System (GBAS) provides differential corrections and ensures the integrity of the navigation solution for aircraft flying precision approaches based on the use of Global Navigation Satellite Systems (GNSS). Operational GBAS ground stations today provide corrections only for the L1 signals of the Global Positioning System (GPS). By design, GBAS provides corrections that are valid and accurate in the vicinity of the ground reference station. However, decorrelation of the ionospheric error typically occurs over distance and can lead to positioning errors for aircraft on approach. This situation can become critical in the presence of significant ionospheric activity, such as the presence of unusually large ionospheric gradients acting between the GBAS ground station and the aircraft on approach. It is therefore essential to monitor for such potentially harmful ionospheric effects and to prevent significant positioning errors during precision approaches. With the introduction of dual-frequency GNSS into GBAS planned for future GBAS approach service types (GAST) (see also Gerbeth et al., (2016)), new monitoring capabilities are emerging and can be exploited.

In recent work in Gerbeth et al., (2022), we proposed a dual-frequency ionospheric monitoring scheme that combines pseudorange corrections from two different frequencies transmitted by the ground station and compares these values with dual-frequency ionospheric delay estimates for each satellite computed at the aircraft. This allows individual satellites with significant residual errors to be excluded from further processing and incorporation into the position and protection level calculations without additional monitoring effort at the GBAS ground station. In addition, monitoring the actual error in the position domain allows all satellites currently in use to be monitored simultaneously, minimizing the computational burden of considering individual subsets of satellites while avoiding strong assumptions about the maximum number of satellites simultaneously affected by an ionospheric disturbance. In addition, position domain monitoring takes advantage of the knowledge of the instantaneous projection factors of range errors into position, improving availability especially in the case of strong geometries with a large number of satellites.

This approach of monitoring the ionosphere based on measurements on two frequencies was subsequently further studied, e.g. by Saito et al., (2022), and adapted by Murphy et al., (2022), to use raw measurements potentially provided by a future GBAS service type in addition to the classical broadcast of corrections. All these adaptations of the monitor so far have in common that they are snapshot-based, looking only at single epochs and estimating the current ionospheric difference and its effect on the user position. In Caamano et al., (2023), we recently evaluated the performance and availability of the monitoring approach for different GBAS processing modes (single-frequency code carrier smoothing, divergence-free code carrier smoothing) as well as for single-constellation GPS and dual-constellation GPS and Galileo scenarios. While overall simulations and tests with real data in this work showed very promising results, especially in case of single constellation scenarios with particularly weak geometries, we found a substantial number of cases where the ionospheric protection levels exceeded the associated alert limit under nominal ionospheric conditions, i.e. without any gradient or anomaly present. The nominal noise alone, in combination with a weak geometry and the stringent requirements in terms of missed detections, lead to considerably large ionospheric protection levels.

To overcome this limitation, we revisit an older idea in the context of ionospheric monitoring for GBAS, especially the Approach Service Type D (GAST D), where a prior probability for the presence of an anomalous ionospheric gradient has been proposed to facilitate the monitoring at the GBAS ground stations and increase the availability of the system. This general idea has been discussed in several publications over the years, such as Felux et al., (2015), Pullen et al., (2017), Patel et al., (2018) and more recently Yoon et al., (2020). These studies typically proposed a fixed, predefined prior probability, typically in the range of 10^{-3} to 10^{-5}, derived for a particular region based on experience and long-term monitoring of the ionospheric activity.

In this work we extend the previously developed dual-frequency ionospheric monitor in position domain to leverage the use of previous ionospheric estimates and derive an instantaneous probability of the presence of an anomalous gradient (rather than always assuming an anomaly to be present). The motivation behind this is that, unlike cycle slips and other instantaneous faults that need to be monitored, ionospheric gradients do not suddenly appear or disappear, but are transient in nature and errors build up over time. The time behavior of the difference between ground and air ionospheric estimates therefore contains additional information that can be exploited. In Section 2, we begin by briefly reviewing the basics of dual-frequency ionospheric monitoring and the potential for improving availability under nominal conditions. We then present two different monitoring approaches aimed at determining whether harmful ionospheric activity is currently present. Section 3 begins with a brief description of the process of adjusting the sensitivity of the proposed new monitors. Afterwards, the detection performance is studied using a large-scale simulated data set, and the estimated probability of ionospheric activity is evaluated using both simulated data and real measurements from a ground installation.

2. METHODS

2.1 Ionospheric Monitoring based on Ionospheric Protection Levels

This section gives a short introduction about the previously introduced (Gerbeth et al., (2022)) ionospheric monitoring concept for dual-frequency GBAS. The core idea is the direct comparison of the experienced ionospheric delay at the ground station and on the airborne user side. The slant ionospheric delay can be estimated at the airborne side by combining smoothed pseudoranges ($\hat{\rho}$) on L1 and L5 frequencies as follows:

$$I_{air,L1,i} = \frac{f_{L5}^2}{f_{L1}^2 - f_{L5}^2} (\hat{\rho}_{L5,i} - \hat{\rho}_{L1,i}) \tag{1}$$

The current ionospheric delay at the ground, I_{ground}, can then be similarly calculated based on available measurements (see Murphy et al., (2021)) or based on received pseudorange corrections as we proposed earlier in Gerbeth et al., (2022). Using these two estimates, we can derive a test statistic that describes the best estimate of the ionospheric delay difference between ground and air as follows:

$$I_{test,\,i} = I_{ground,\,i} - I_{air,i} - median(\{I_{ground,\,j} - I_{air,j}\}_{j \in S_C}), \tag{2}$$

where $I_{ground,j}$ and $I_{air,j}$ refer to the ionospheric estimate for satellite j within all satellites belonging to a constellation (S_C). While when projecting into position domain, common biases on I_{test} are not relevant, we will later on utilize these range domain estimates to monitor for activity, hence the need to remove the median bias per constellation. Based on $I_{test,\,i}$ and the known satellite geometry, as well as the monitoring noise, we can derive a so-called ionospheric protection level which can then be compared with a corresponding monitoring threshold to allow exclusion of affected satellites or to trigger a switch to an ionosphere-free processing mode, as described in Caamano et al., (2023):

$$VPL_{iono} = \left|\sum_{i=1}^{N}\left(I_{test,i} \cdot s_{vert,i}\right)\right| + k_{md,\,iono} \cdot \sqrt{\sum_{i=1}^{N} \sigma^2_{monitor,i} \cdot s^2_{vert,i}} \leq \mathrm{E}_{\mathrm{v,\,iono}}\,. \tag{3}$$

The projection factor $s_{vert,i}$ describes the projection from range domain into the vertical axis of the position domain (in approach coordinates) and depends on the local satellite geometry and the glide path angle of the approach. The monitoring noise ($\sigma^2_{monitor}$) for satellite i includes all ground and airborne noise and multipath contributions affecting the ionospheric monitoring. For details, we refer to Murphy et al., (2022). Finally, the inflation factor $k_{md,\,iono}$ depends on the desired residual integrity risk (P_{IR}) based on the inverse Q-function as follows:

$$k_{md} = Q^{-1}(0.5 \cdot P_{IR}). \tag{4}$$

As we introduced in Section 1, earlier studies like Yoon et at., (2020) had proposed to account for a prior probability of occurrence of anomalous ionospheric gradients to relax the requirements on the monitoring. In this work, instead of introducing a fixed, predefined prior probability based on analysis of historic data for a given region, we propose to dynamically estimate the probability of the presence of any ionospheric disturbance (p_{iono}) based on real-timemeasurements available at the airborne GBAS user. Thus, Equation (3) becomes:

$$VPL_{iono} = \left|\sum_{i=1}^{N}\left(I_{test,i} \cdot s_{vert,i}\right)\right| + Q^{-1}\left(\frac{0.5 \cdot P_{IR}}{p_{iono}}\right) \cdot \sqrt{\sum_{i=1}^{N} \sigma^2_{monitor,i} \cdot s^2_{vert,i}}\,, \tag{5}$$

with a resulting inflation factor for the monitoring noise component depending on the current estimated probability of an ionospheric threat being present. A number of different metrics can be considered to estimate this probability based on instantaneous measurements available to the airborne user but also previous epochs. In position domain, for example the magnitude and rate of the projection of the ionospheric differences (left part of Equation (5)) indicate changes in the ionosphere, but prove to be less reliable, as the projection factors potentially cause some errors to compensate each other – a property that is actually beneficial for the overall monitoring approach. In range domain on the other hand, a multitude of tests can be performed, monitoring rates and magnitudes of the individual values of I_{test} or looking at a certain window of past estimates. Even classical CCD-like (code carrier divergence) metrics, as described in Simili & Pervan, (2006), are conceivable, when adapted to be sufficiently sensitive.

This is because typical ionospheric threats such as gradients are persistent effects over at least a few minutes and do not appear or disappear within single epochs. This characteristic can be exploited in monitoring, in contrast to, for example, cycle slips, which occur instantaneously without prior warning. During the course of this study, a number of metrics were tested and a combination of two complementary metrics was ultimately used, as described in the following two subsections.

2.2 Monitoring for Ionospheric Activity Based on Magnitude of I_{test}

The first metric looks at the magnitude of the individual ionospheric differences. For the current epoch, we sum the magnitude of all $I_{test,i}$, reduced by a fixed bias b_{mag}, which serves as a parameter for tuning sensitivity. To be independent of the number of currently available satellites, N, the result is normalized, yielding a test result as follows:

$$T_{mag} = \frac{1}{N}\sum_{i} \max(0,\ |I_{test,i}| - b_{mag}). \tag{6}$$

This resulting test metric is then directly translated into a probability for activity based on the following relation:

$$p_{iono,Tmag} = \begin{cases} p_{min}\ , & \text{for } \mathrm{T_{mag}} = 0 \\ 1\ , & \text{for } \mathrm{T_{mag}} > \mathrm{T}_{thresh} \\ 10^{\log_2(\mathrm{T}/\mathrm{T}_{thresh})}\ , & \text{otherwise} \end{cases} \tag{7}$$

In this case, p_{min} is the minimum prior probability and has to be predefined, for example, as mentioned above, based on historical measurements, potentially depending on the activity of a region or known seasonal variations. In the remaining part of this work, we used a value of 10^{-3} as was proposed in earlier studies for example by Yoon et al., (2020). The parameter T_{thresh} is another design parameter that influences the missed detection rate (sensitivity) of the test. In Section 3 we will elaborate further on these two design parameters and their effect on sensitivity.

2.3 Monitoring for Ionospheric Activity Based on Range Domain Cumulative Sums

The second metric we utilize for activity detection is based on cumulative sum monitoring (CUSUM) of the rate of the test statics $I_{test,i}$. This test, originally introduced by Page, (1954), allows to detect changes in the empirical properties of a noisy time series. For details on the test itself and its properties, we refer to the original publication. In our application, we want to monitor the rate of $I_{test,i}$ as defined in Equation (8), where Δt refers to the sample interval.

$$\Delta I_i(n) = \frac{I_{test,i}(n) - I_{test,i}(n-1)}{\Delta t} \tag{8}$$

Based on the current rates ΔI_i, for each satellite, two running sums (a *high* and a *low* sum) are computed as given in Equation (9). Again, we have a design parameter that allows for adjusting the sensitivity of the test: b_r can be considered related to the nominal rate at which we expect $I_{test,i}$ to change over time while satellites are moving. Typically, the rate of $I_{test,i}$ will contain nominal biases, as for example the signal in space from the satellite to the user will pass through different parts of the ionosphere at slightly different angles, causing minor but systematic differences in the slant ionospheric delays.

$$\begin{aligned} S_{H,i}(n) &= \max\{0,\ \ S_{H,i}(n-1) + \Delta I_i(n) - b_r\} \\ S_{L,i}(n) &= \max\{0,\ \ S_{L,i}(n-1) - \Delta I_i(n) - b_r\} \end{aligned} \tag{9}$$

The final metric for the CUSUM based test is obtained by finding the overall maximum of both of the running sums for all satellites currently monitored:

$$T_{rCUSUM}(n) = \max_i\{S_{H,i}(n),\ \ S_{L,i}(n)\}. \tag{10}$$

Subsequently, similar to the previous test, we derive a test-specific probability for activity from T_{rCUSUM} as follows:

$$p_{iono,rCUSUM} = \begin{cases} p_{min}\ , & \text{for } \mathrm{T}_{rCUSUM} = 0 \\ 1\ , & \text{for } \mathrm{T}_{rCUSUM} > \mathrm{T}_{thresh} \\ 10^{\log_2(\mathrm{T}/\mathrm{T}_{thresh})}\ , & \text{otherwise} \end{cases} \tag{11}$$

Again, with T_{thresh} we have a second parameter that allows us to control the test sensitivity. As a final step in the overall monitoring, the two individual probabilities based on the two independent tests (the one computed in Section 2.2 and the one computed in Section 2.3) are combined, simply by taking the maximum of both. The resulting p_{iono} is considered as the current probability of any anomalous ionospheric activity acting between the GBAS user and the ground station and it is used in Equation (5) to calculate the instantaneous VPL_{iono}.

$$p_{iono} = \max\left(p_{iono,\ Tmag}, p_{iono,\ \mathrm{rCUSUM}}\right) \tag{12}$$

3. RESULTS AND DISCUSSION

3.1 Design Goals and Sensitivity Analysis

Both detection techniques we described in Section 2 incorporate two parameters to adjust their sensitivity, i.e. missed detection rate and false alarm rate. In this context, we define missed detections as cases where the probability for activity (p_{iono}) did not reach a value of 1 before the original ionospheric monitoring based on Equation (3) would have exceeded the monitoring threshold. In other words, in all cases where the monitoring would cause any satellite to be excluded or trigger a switch to an ionosphere-free processing mode, it should not be affected or even delayed. Consequently, Equation (3) shall restored to the desired residual integrity risk at or before the occurrence of a detection.

We used a test dataset further described in the following subsection to find an optimal set of parameters for both techniques and assess the achieved results obtained by varying the parameters as well as applying them for detection on different data. For illustrative purposes and to facilitate the interpretation of the results presented in the following sections, **FIGURE 1** shows the relationship between the number of missed detections within a test data set and the two design parameters introduced earlier, in this case for the magnitude test described in Section 2.2. The red line in the figure illustrates the parameter pairs (in this case for the total iono magnitude test) that will be used later when presenting the results. We call a combination of two parameter pairs (for the two proposed detectors) sensitivity level in the following results. **TABLE 1** contains the parameter values for some selected sensitivity levels as well as the general formulas for calculation.

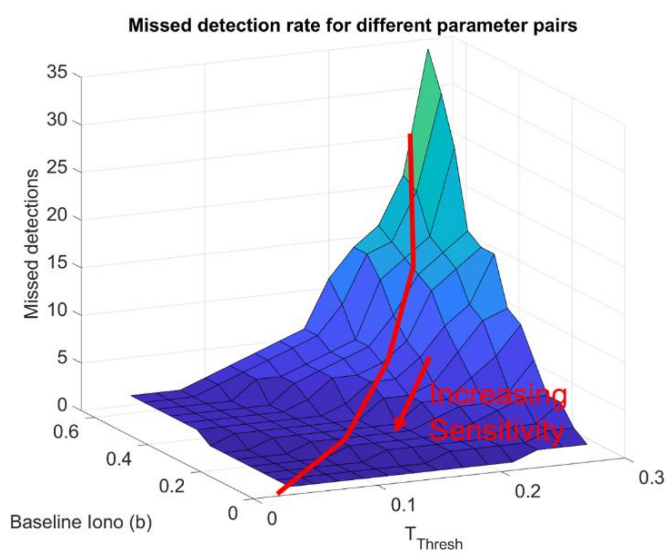

FIGURE 1 Exemplary sensitivity study for the ionospheric difference magnitude test based on simulated data set. Results in Sections 3.2 and 3.3 are presented along the red line indicated in parameter space.

TABLE 1

Parameters associated with the sensitivity levels 4, 8 and 12 in **FIGURE 2** and **FIGURE 4**, and additionally the formula to derive each parameter values for a given sensitivity level S.

Parameter	Sensitivity 4	Sensitivity 8	Sensitivity 12	Sensitivity S
b_{mag}	0.5	0.3	0.1	$0.7 - S \cdot 0.05$
$\mathrm{T}_{thresh,\,mag}$	1.4	0.8	0.2	$2 - S \cdot 0.15$
b_r	28×10^{-4}	16×10^{-4}	4×10^{-4}	$4 \cdot 10^{-3} - S \cdot 3 \cdot 10^{-3}$
$\mathrm{T}_{thresh,\,rCUSUM}$	0.47	0.27	0.07	$0.67 - S \cdot 0.05$

3.2 Assessing Detection Capability

The first aspect we want to look at, is the ability to detect any anomalous ionospheric effects and irregularities in a timely manner, to ensure that the detections of the actual ionospheric monitor's detections are not delayed or even prevented when there is indeed anomalous activity. To evaluate this property, we used a large simulated data set generated for our most recent work in Caamano et al., (2023). In this simulation, a total of nearly 80000 approaches were simulated for single constellation GPS as well as GPS and Galileo combined, taking into account noise and multipath performance according to an MLA (multipath limiting antenna) GBAS ground station performance, and AAD-B airborne models. Approximately 46000 of the simulated trajectories contained simulated anomalous ionospheric gradients of varying strength. For a more detailed description of the noise and multipath assumptions, and the ionospheric perturbations introduced, we refer to the original publication from Caamano et al., (2023). From this total data set, we selected 15000 approach trajectories using only GPS under active ionospheric conditions to evaluate the detection capability of the activity monitoring.

FIGURE 2 shows the results across different levels of sensitivity (see **TABLE 1** for the associated parameters), both for the combined detector and for the two individual monitoring metrics for illustrative purposes. As described earlier, we define a missed or late detection as a situation where p_{iono} (or $p_{iono,\,\mathrm{rCUSUM}}$ and $p_{iono,\,\mathrm{Tmag}}$ respectively for the red and yellow lines in **FIGURE 2**) did not reach a value of 1 before an ionospheric irregularity would have been detected with the original monitoring condition in Equation (3). As expected, the missed or late detections decrease with increasing sensitivity for both individual detections, but show slightly different behavior for each. In addition, we find that the combined metric (blue) is significantly below the individual detectors across all sensitivities, showing complementary behavior, i.e. apparently detecting different types of anomalous irregularities. At a sensitivity level between 7 and 8, there are no missed detections left in the test set of 15000 approaches. The right side of **FIGURE 2** additionally gives some indications about the time delay between the detection of activity ($p_{iono} = 1$) and the moment when VPL_{iono} exceeded the alert limit. In this case, negative time delays are desirable, indicating that p_{iono} reached a value of 1 earlier than VPL_{iono} triggering an alarm.

For a sensitivity of 8, where there were no more missed detections present in the data set used, we additionally show the histogram of time delays in **FIGURE 3**. While in some cases an activity is detected significantly before the onset of a harmful error, partly due to false positive detections, we generally see an increase towards the time when an irregularity actually caused the ionospheric monitor to trigger an alarm. In the last seconds before the trigger, we see a sharp drop, indicating that most irregularities are detected with some margin. Of note is the spike right at a time delay of 0 in the plot. In these cases, a gradient between ground and air was already present at the start of a simulated approach and was immediately detected by the ionospheric activity monitor, while in the same epoch causing VPL_{iono} from the actual ionospheric monitor to also trigger, resulting in a delay of 0 seconds between the two.

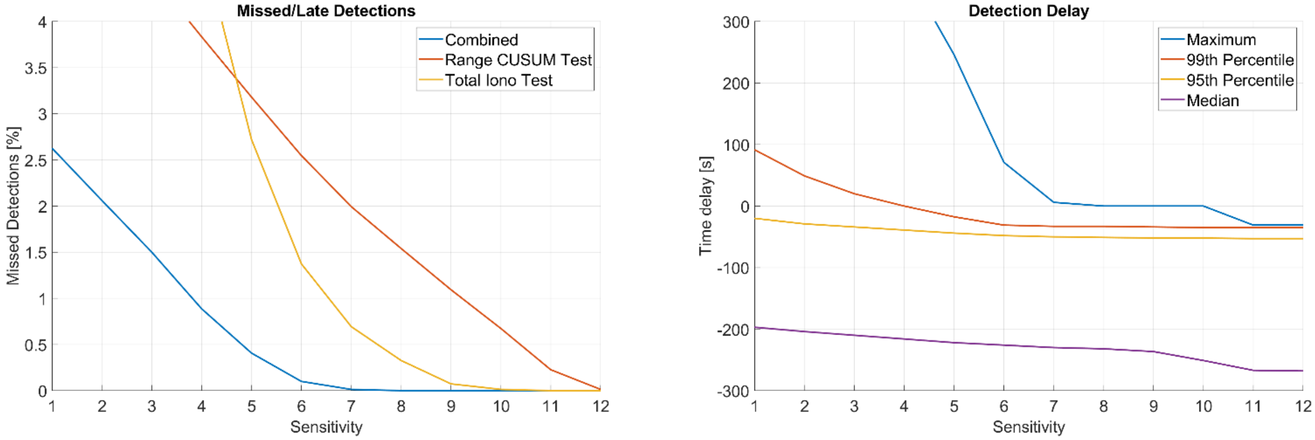

FIGURE 2 Percentage of missed or late detection for a changing monitoring sensitivity (left) and the delay between the moment where p_{iono} reached 1 and the moment VPL_{iono} triggered an alarm (right).

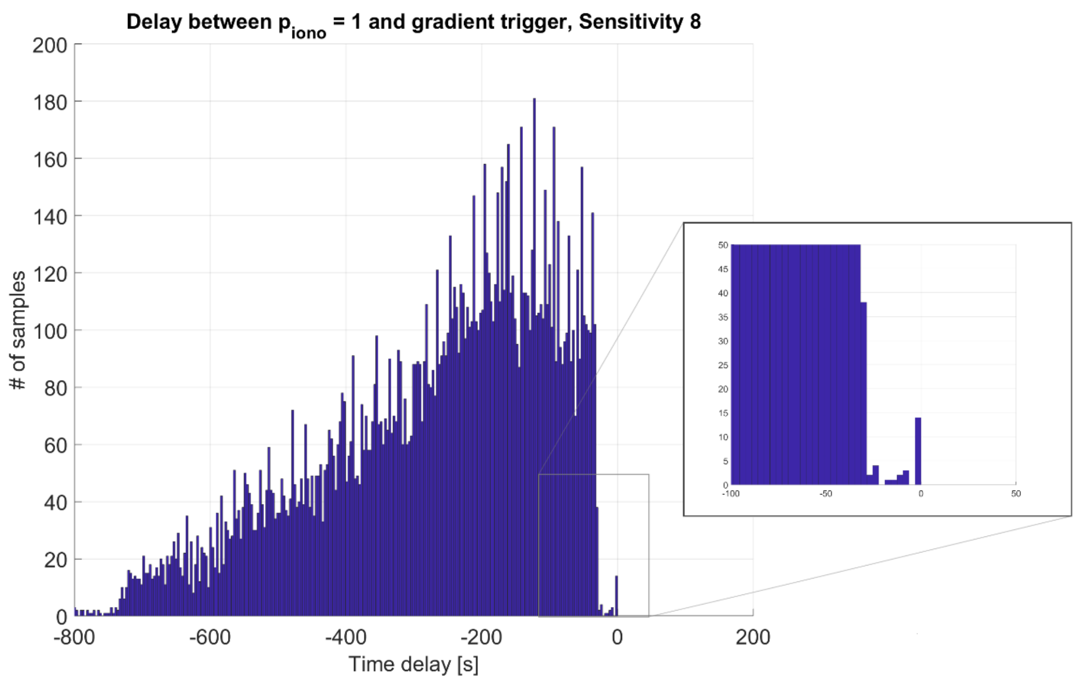

FIGURE 3 Histogram of time delays related to the results shown for sensitivity 8 in **FIGURE 2**.

3.3 Assessing Nominal Performance Improvements

While in the previous section only the detection capability was evaluated, the real benefit of the proposed approach would only emerge under nominal conditions. Therefore, it is necessary to evaluate how the estimated probabilities of ionospheric activity behave at different levels of sensitivity, but also when applied to a real data set.

First, we want to look again at simulated approaches. From the previously described set of 80000 simulated approaches, in this case we selected 9000 without the presence of any simulated ionospheric disturbance, as before for a GPS-only constellation. The left plot in **FIGURE 4** shows the average achieved p_{iono} over the same sensitivity scale as used before. As we can see, at a sensitivity level of 8, where we previously found that we were able to correctly detect all cases of activity, we can still achieve a median p_{iono} of about $3 \cdot 10^{-3}$, showing some potential for reducing the nominal ionospheric protection levels. While in this case, the nominal noise and multipath present in the data were simulated and thus were potentially more favorable than in real measurements, we used the same setup to analyze 24 hours of data collected in a ground installation. In this case, the measurements were collected with two choke ring antennas, separated by about 1.5 km and located in central Germany, thus assuming a generally calm ionosphere without significant irregularities. After applying the monitoring with exactly the same sensitivity levels, the resulting probabilities are presented in the right-side plot of **FIGURE 4**. As expected, in this scenario with worse antennas (and siting) compared to MLAs in a typical GBAS installation and thus considerably higher multipath errors compared to the simulated data, we find higher average p_{iono} at the same sensitivity levels, but still indicating potential for improvements in nominal conditions around a sensitivity level of 8.

In particular when looking at the time series, we can find longer periods of up to 20 minutes where there are no false detections of activity, thus allowing for a reduction of nominal ionospheric protection level. A snapshot of the full 24 hours analyzed is shown in **FIGURE 5**, indicating the change in estimated p_{iono} over time. When compared to the simulated results, this set of measurements typically shows spikes in p_{iono} when individual low-elevation satellites experienced stronger multipath errors for at least one of the two receivers, causing fluctuations especially in the CUSUM-based test.

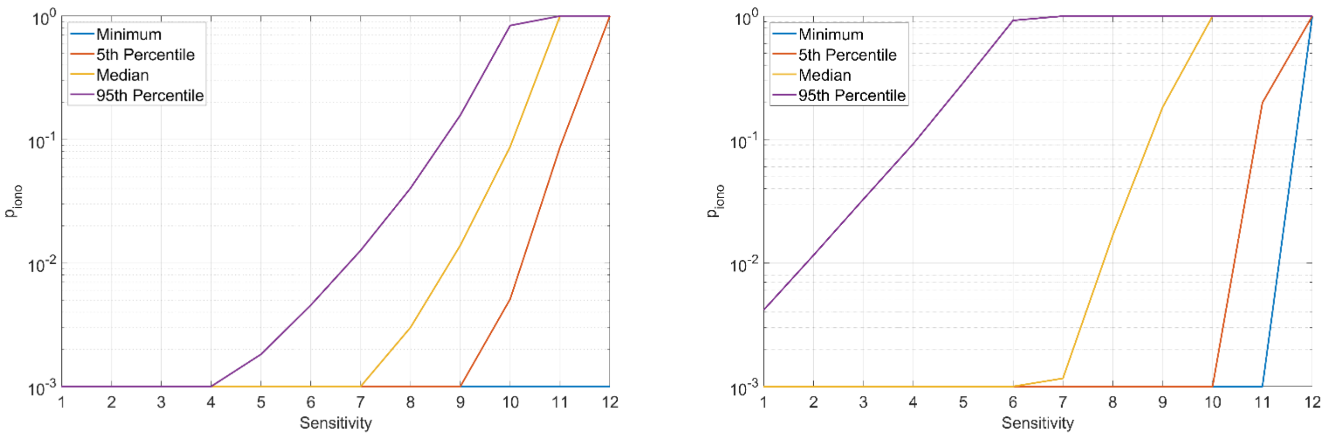

FIGURE 4 Resulting probability of ionospheric activity for different sensitivity levels for 9000 simulated approaches (left) and for 24 hours of data collection with a ground installation based on choke ring antennas (right).

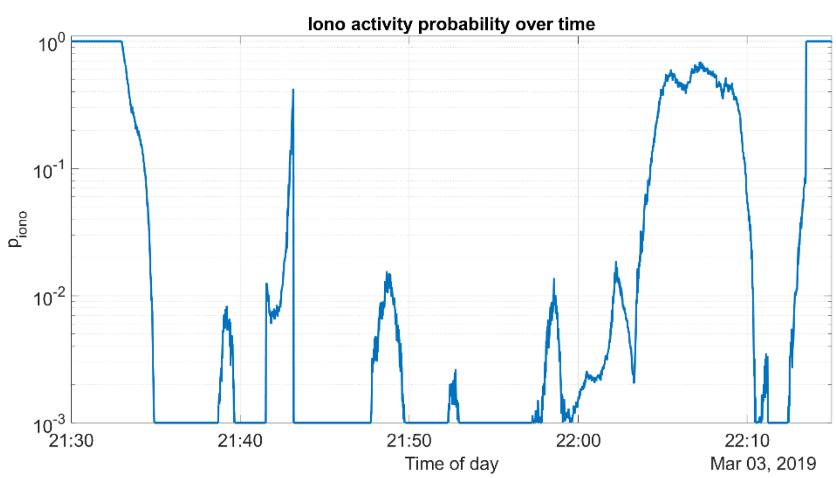

FIGURE 5 Time series of the probability of ionospheric activity using detection parameters according to sensitivity level 8 and applied to measurements taken from two choke ring antennas in a ground installation.

4. CONCLUSIONS AND FUTURE WORK

In this study, we have demonstrated the effectiveness of combining two ionospheric monitoring metrics to distinguish between active and calm ionospheric conditions using measurements available on board an aircraft in future dual-frequency GBAS. Our results indicate that all simulated gradients can be reliably detected when adjusted for a given hardware performance, including ground and airborne noise and multipath effects.

This opens up the possibility of reducing ionospheric protection levels during certain phases of flight under nominal conditions, potentially increasing the efficiency of ionospheric threat mitigation strategies. Particularly in single constellation scenarios or in general with a low number of available satellites, availability could be increased in this way, as previous studies have shown a limited margin between the achieved ionospheric protection levels and the desired alert limits in such cases. Our investigations showed the benefits of employing longer smoothing time constants and divergence-free processing techniques to reduce the effects of multipath and noise, but also to preserve the dynamics of ionospheric effects without distortions induced by single-frequency code-carrier smoothing.

In future work, it is crucial to evaluate the performance of the proposed methodology using different hardware configurations and under different anomalous conditions. This should ensure the robustness and reliability of the approach in a wide range of scenarios and potentially adapt it to additional applications such as urban air mobility. In addition, future studies should focus on the systematic evaluation of detection delays for simple ionospheric gradients. Understanding the detection delay of these gradients is essential for refining monitoring and mitigation strategies, particularly in aviation applications with stringent time-to-alert requirements.

5. REFERENCES

Caamano, M., Gerbeth, D., Sato, H., Circiu, M.-S., & Felux, M. (2023). Performance Evaluation of the Ionospheric Threat Mitigation Strategies in Dual-Frequency Multi-Constellation GBAS. *2023 IEEE/ION Position, Location and Navigation Symposium (PLANS)*, (pp. 196-207). Monterey, CA, USA. doi:10.1109/PLANS53410.2023.10140062

Felux, M., Lee, J., & Holzapfel, F. (2015). GBAS ground monitoring requirements from an airworthiness perspective. *GPS Solutions, 19*, pp. 393-401. doi:10.1007/s10291-014-0398-0

Gerbeth, D., Caamano, M., Circiu, M.-S., & Felux, M. (2022). Airborne Ionospheric Gradient Monitoring for Dual-Frequency GBAS. *Proceedings of the 2022 International Technical Meeting of The Institute of Navigation.*

Gerbeth, D., Circiu, M.-S., Caamano, M., & Felux, M. (2016). Nominal performance of future dual frequency dual constellation GBAS. *International Journal of Aerospace Engineering*.

Lee, J., Nam, G., Min, D., Sun, A., & Pullen, S. (2023). Network-Based Augmentation System (NBAS) Architectures Optimized to Support Urban Air Mobility (UAM). *Proceedings of the 2023 International Technical Meeting of The Institute of Navigation*, (pp. 441-453). Long Beach, California.

Murphy, T., Harris, M., Balvedi, G., McGraw, G., Wichgers, J., Lavik, L., . . . Saito, S. (2022). Ionospheric Gradient Monitoring for Dual Frequency Multi-Constellation GBAS. *Proceedings of the 2022 International Technical Meeting of The Institute of Navigation*, (pp. 1075 - 1097). Long Beach, California. doi:10.33012/2022.18178

Murphy, T., Harris, M., McGraw, G., Wichgers, J., Lavik, L., Topland, M., . . . Saito, S. (2021). Alternative Architecture for Dual Frequency Multi-Constellation GBAS. *Proceedings of the 34th International Technical Meeting of the Satellite Division of The Institute of Navigation (ION GNSS+ 2021)*, (pp. 1334 - 1374). St. Louis, Missouri. doi:10.33012/2021.18152

Page, E. S. (1954). Continuous Inspection Schemes. *Biometrika, 41*(1-2), 100-115. doi:10.1093/biomet/41.1-2.100

Patel, J., Khanafseh, S., & Pervan, B. (2018). Spatial Gradient Monitor for GBAS. *IEEE/ION Position, Location and Navigation Symposium (PLANS)*, (pp. 571-582). Monterey, CA. doi:10.1109/PLANS.2018.8373429

Pullen, S., Cassell, R., Johnson, B., Brenner, M., Weed, D., Cypriano, L., . . . Dennis, J. (2017). Impact of Ionospheric Anomalies on GBAS GAST D Service and Validation of Relevant ICAO SARPs Requirements. *Computer Science*. doi:10.33012/2017.15135

Saito, S., Yoshihara, T., Murphy, T., Harris, M., Balvedi, G., McGraw, G., . . . Tuffaha, M. (2022). Validation of Ionospheric Anomaly Monitor for DFMC GBAS under Disturbed Ionospheric Conditions. *Proceedings of the 35th International Technical Meeting of the Satellite Division of The Institute of Navigation (ION GNSS+ 2022)*, (pp. 3150-3159). Denver, Colorado, USA. doi:10.33012/2022.18355

Simili, D. V., & Pervan, B. (2006). Code-Carrier Divergence Monitoring for the GPS Local Area Augmentation System. *2006 IEEE/ION Position, Location, And Navigation Symposium*, (pp. 483-493). Coronado, CA, USA.

Yoon, M., Lee, J., & Pullen, S. (2020). Integrity risk evaluation of impact of ionospheric anomalies on GAST D GBAS. *NAVIGATION, 67*(2), pp. 223-234. doi:10.1002/navi.339